Transition Effects on Slender Vehicle Stability and Trim Characteristics

LARS E. ERICSSON*
Lockheed Missiles and Space Company, Inc., Sunnyvale, Calif.

The effect of boundary-layer transition on high-performance re-entry bodies has been studied extensively. A great volume of experimental results has become recently available for the combined effects of crossflow and nose bluntness on the transition on slender cones, both with and without mass addition. The results of a correlation study of these new transition data are reported elsewhere. In the present paper the correlation results are used to determine the effects of transition on slender vehicle stability and trim characteristics. The coupling effects from symmetric nose bluntness and associated entropy swallowing are considered in detail. A limited discussion of the effects (on trim) of asymmetric nose bluntness is also provided. The adverse effects of transition, both in regard to stability and trim characteristics, are of some concern for a ballistic re-entry vehicle. Provided that critical nose bluntness-cone angle combinations giving negative damping are avoided, the effect of transition for lifting re-entry is mainly a change of body trim, a change which in magnitude might be well within the available control capability.

Nomenclature

A	= body surface area
c	= reference length (cone base diameter, d_B)
d	= body diameter
D_N	= nose drag, coefficient $C_{DN} = D_N/(\rho_\infty U_\infty{}^2/2)(\pi d_N{}^2/4)$
k, K	= proportionality constants
l	= sharp cone body length
$\dot{m}$	= rate of ablative mass addition, coefficient $Cq = (\partial\dot{m}/\partial A)/\rho_e U_e$
M	= Mach number
M_p	= pitching moment, coefficient $C_m = M_p/(\rho_\infty U_\infty{}^2/2)Sc$
N	= normal force, coefficient $C_N = N/(\rho_\infty U_\infty{}^2/2)S$
n_1	= Mangler-parameter, Eq. (3)
p	= static pressure, coefficient $C_p = (p-p_\infty)/(\rho_\infty U_\infty{}^2/2)$
q	= rigid body pitch rate
r	= body radius
R_l	= Reynolds number based on sharp cone length
S	= reference area $S = \pi c^2/4$
t	= time
T	= temperature
Δt	= viscous timelag
U	= axial velocity
x	= axial body coordinate from sharp cone apex
x_0	= start of conic frustum on blunted cone
α, α_0	= angle of attack and trim angle of attack, respectively
$\tilde{\alpha}$	= effective local flow inclination
δ, δ^*	= boundary layer thickness and boundary layer displacement thickness, respectively
Δ	= difference
θ	= local body attitude
θ_c	= cone half-angle
ν	= Prandtl-Meyer angle
ξ	= dimensionless axial coordinate, $\xi = x/c$
τ	= thermolag of ablation response
ω	= angular pitch rate
$\bar{\omega}$	= reduced frequency, $\bar{\omega} = \omega c/U_\infty$
ρ	= air density
χ	= hypersonic similarity parameter
χ_l	= hypersonic scaling parameter $\chi_l{}^{-1} = 2C_{DN}{}^{1/2}(d_N/d_B)/\theta_c$

Subscripts

a, a_0	= due to ablation and steady state ablation, respectively
AC	= aerodynamic center
AT	= asymmetric transition front
AW	= adiabatic wall
B, N	= base and nose, respectively
c.g.	= center of gravity
e	= edge of boundary layer
EW	= entropy wake impingement
i	= inviscid flow
LW, WW	= leeward and windward side, respectively
$LAM, TURB$	= laminar and turbulent boundary layer, respectively
R	= recovery
ST	= stagnation
TR	= transition
W	= wall condition
0	= $\alpha = 0$ or $d_N = 0$
1	= forebody lumped load station for crossflow effect
∞	= freestream conditions

Superscripts

i	= induced, e.g., $\Delta^i C_{NTR}$ = change in (aft body) normal force due to transition
-	= barred symbols denote mean values

Derivative Symbols

$\dot{\alpha}$	$= \partial\alpha/\partial t$; $\dot{m} = \partial m/\partial t$
$C_{N\alpha}$	$= \partial C_N/\partial\alpha$; $C_{m\theta} = \partial C_m/\partial\theta$
C_{mq}	$= \partial C_m/\partial(cq/U_\infty)$; $C_{m\dot{\alpha}} = \partial C_m/\delta(c\dot{\alpha}/U_\infty)$
$C_{m\dot{\theta}}$	$= C_{mq} + C_{m\dot{\alpha}}$
$C_{\bar{m}\bar{\theta}}$ and $C_{\bar{m}\dot{\bar{\theta}}}$	= effective integrated mean values

Introduction

MOTION anomalies of re-entering high-performance missiles have been observed at the time when boundary-layer transition is known to have started to occur on the vehicle (aft body). It is true that peak heating and peak dynamic pressure often also occur close to the time of transition, and these events could by themselves be responsible for the anomalies. However, even after careful screening, the fact remains that boundary-layer transition initiates defects in both stability and trim characteristics—defects that can be amplified greatly during the following peak heating and peak dynamic pressure portions of the trajectory.

Unless otherwise stated, the boundary-layer transition effects discussed in the present paper all concern aft body transition; i.e., the mean position of the transition line is located aft of the

Presented as Part II of AIAA Paper 73-126 at the AIAA 11th Aerospace Sciences Meeting, Washington, D.C., January 10–12, 1973; submitted April 13, 1973; revision received September 6, 1973. The author is indebted to R. L. Nelson, G. T. Chrusciel, and J. P. Reding for many enlightening discussions and helpful suggestions.

Index categories: Boundary Layer Stability and Transition; Supersonic and Hypersonic Flow; Entry Vehicle Dynamics and Control.

* Consulting Engineer. Associate Fellow AIAA.

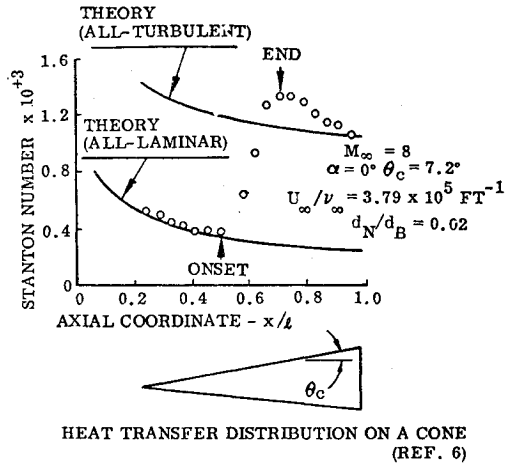

Fig. 1 Overshoot of turbulent heating level in a region of boundary-layer transition.

body c.g. The discussion is also limited to the hypersonic and high supersonic speed ranges.

Transition Effects on Stability Characteristics

The early concern was the effect of so-called symmetric transition, i.e., the effect of increased aft body heating on an ablating body when transition moves forward of the base.[1-3] Later it was shown that, in addition to this effect of symmetric transition, the effect on vehicle stability of asymmetric transition, i.e., the skewing of the transition front, was possibly even stronger.[4-6] The effects are discussed again in the present paper in light of the latest information.[6-13]

Symmetric Transition

When boundary-layer transition occurs forward of the base on an ablating re-entry body, the rate of ablative mass addition is raised dramatically. For symmetric transition, i.e., disregarding the tilting of the transition front with angle of attack, the effect is that on the aft portion of the vehicle the ablative heat shield is in a much hotter (turbulent) environment and, consequently, has a much higher mass addition rate than the rest of the vehicle (Fig. 1). The increased boundary-layer displacement thickness due to mass addition induces (local) pressures that can be expressed as follows for moderate ablation rates[3,14]

$$\Delta C_{pa} = 2\Delta v_a (M_e^2 - 1)^{-1/2} \tag{1}$$

If one assumes a stepwise change from laminar to turbulent heating levels (which is not a bad approximation according to the data shown in Fig. 1) Δv_a is simply the increase of the displacement-thickness-slope $\partial\delta^*/\partial x$ due to mass addition in a turbulent boundary layer. If the mass addition rates are moderate ($C_q < 0.01$) the boundary-layer shape parameter can be assumed to remain unchanged, and one can get the following simple expression[15] (with error being less than 3%)

$$\Delta v_a = K_a C_q \tag{2}$$

The proportionality constant K_a is dependent upon boundary-layer edge conditions and injectant characteristics. For air injection[15] K_a is

$$K_a = 16 n_1 (R_{xTR})_e^{0.2} (T_e/T_{\text{ref}})^{-0.65} (\partial\delta^*/\partial x)_{Cq=0} \tag{3}$$

where $n_1 = 1$ and $n_1 = 0.512$ for flat plate and cone, respectively. The angle-of-attack dependence of C_q can be expressed in linearized form†

$$C_q(t) = C_{q0} + C_{q\alpha}\tilde{\alpha}(t-\tau) \tag{4}$$

$\tilde{\alpha}$ is the generalized angle of attack

$$\tilde{\alpha} = \alpha_0 + \theta + (\xi - \xi_{c.g.})\frac{c\dot{\theta}}{U} \tag{5}$$

The thermodynamic timelag τ is, for convenience, expressed in the following dimensionless form

$$\tau = \xi_\tau c/U \tag{6}$$

For harmonic oscillation, $\theta(t) = \Delta\theta\, e^{i\omega t}$, $\theta(t-\tau) = e^{-i\omega\tau}\theta(t)$, and $\dot{\theta}(t-\tau) = e^{-i\omega\tau}\dot{\theta}(t)$. For small mass addition rates and large thermodynamic timelags the effect of mass addition on the static stability is small compared to the effect on dynamic stability, and the frequency can be assumed to remain constant. This is often the realistic case.[3] Then $\dot{\theta}(t) = \Delta\theta i\omega\, e^{i\omega t} = i\omega\theta(t)$, and one can express $C_q(t)$ as follows:

$$C_q(t) = C_{q0} + C_{q\alpha}\alpha_0 + C_{q\alpha}[\cos(\bar{\omega}\xi_\tau) + \bar{\omega}(\xi - \xi_{c.g.})\sin(\bar{\omega}\tau)]\theta - C_{q\alpha}\{\sin(\bar{\omega}\xi_\tau)/\bar{\omega}] - (\xi - \xi_{c.g.})\cos(\bar{\omega}\xi_\tau)\}(c\dot{\theta}/U) \tag{7}$$

For the hypersonic speeds existing at time of transition on high-performance re-entry bodies, the reduced frequency is very small, $\bar{\omega} \ll 0.01$. Thus, Eq. (7) can for reasonable thermolags (i.e., for $\xi_\tau < 100$) be approximated as

$$C_q(t) = C_{q0} + C_{q\alpha}\alpha_0 + C_{q\alpha}\theta - C_{q\alpha}[\xi_\tau - (\xi - \xi_{c.g.})](c\dot{\theta}/U) \tag{8}$$

The local normal force due to ablation can then be written as follows:

$$\left.\begin{aligned} \Delta C_{Na} &= \Delta C_{Na0} + \Delta C_{Na\theta}\theta + \Delta C_{Na\dot{\theta}}\frac{c\dot{\theta}}{U_\infty} \\ \Delta C_{Na\theta} &= \Delta C_{Na\alpha} \\ \Delta C_{Na\dot{\theta}} &= -\Delta C_{Na\alpha}[\xi_\tau - (\xi - \xi_{CG})]/(U/U_\infty) \end{aligned}\right\} \tag{9}$$

Usually $\xi_\tau^2 \gg (\xi - \xi_{c.g.})^2$, and for sharp slender cones $U \approx U_\infty$. Thus

$$\Delta C_{Na\dot{\theta}}/\Delta C_{Na\theta} \approx -\xi_\tau \tag{10}$$

That is, the ablation-induced aft body normal force will be statically stabilizing but dynamically destabilizing. This behavior has been observed in wind tunnel tests‡ using low-temperature sublimers§ for simulation of heat shield ablation.[2,17] As the transition line moves forward, the effects of boundary-layer crossflow and a shielding (reradiating) shear layer complicate

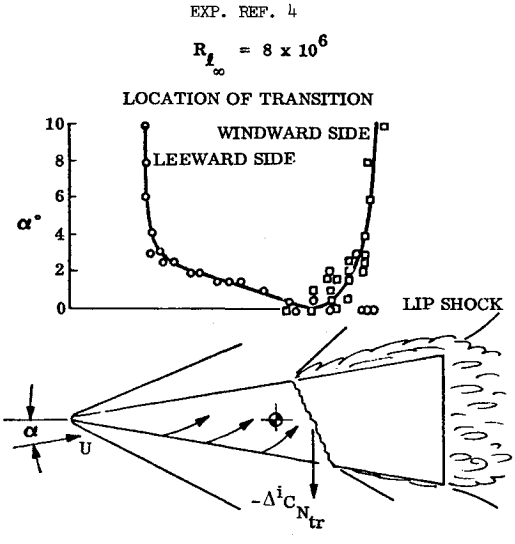

Fig. 2 Effect of angle of attack on boundary-layer transition on a 10° sharp cone at $M_\infty = 6$.

† It is assumed that the mass addition rate is a linear function of the heating rate and lags it by a constant time increment τ; i.e., nonlinear transients in the ablation process are not considered.

‡ Many other tests have shown the same results, but they have not been published in the open literature.

§ Although these materials are not insensitive to the ambient (back) pressure.[16]

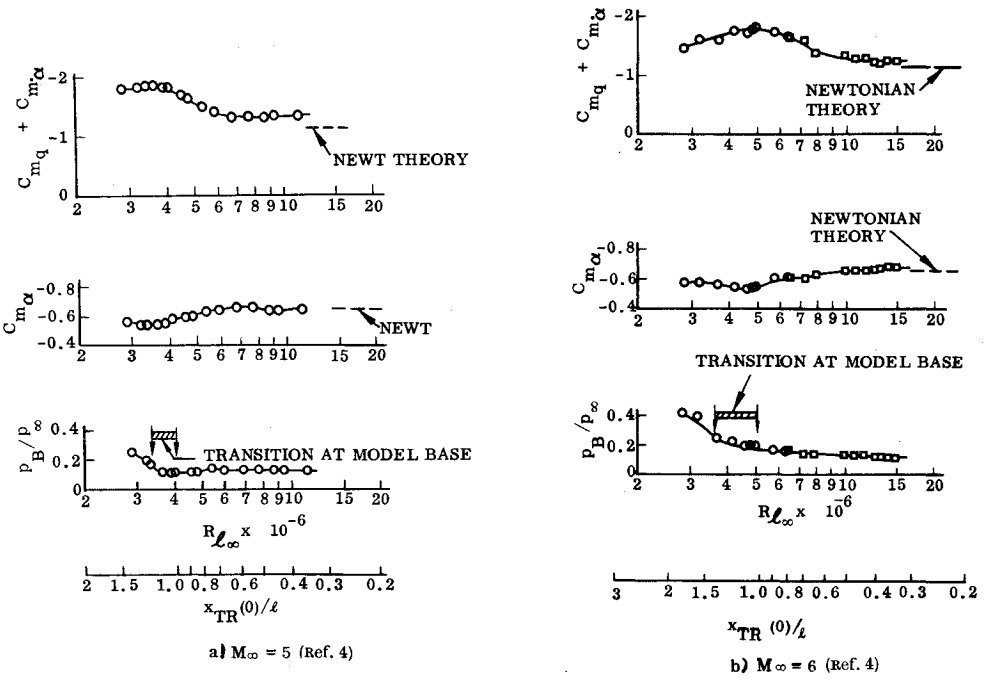

Fig. 3 Effect of Reynolds number on dynamic and static stability.

the analysis. The ablation effect can then be damping or undamping, depending upon distribution along the vehicle of mass addition rates and thermo timelags.[3,18,19]

Asymmetric Transition

It does not take more than a casual look at the asymmetric transition results presented by Ward[4] (Fig. 2) to realize that the symmetric transition effects discussed in the previous section may be rather insignificant compared to the effects of asymmetric transition on stability and trim characteristics of slender cones. The difference in self-induced pressure for turbulent and laminar flow is apparently enough to cause substantial changes in the vehicle stability characteristics (Fig. 3). Using the same stepwise change from laminar to turbulent boundary-layer conditions discussed in the previous section, the loads induced through asymmetric transition can be expressed as follows:

$$\left.\begin{aligned}
\Delta^i C_{NTR} &= (\Delta^i C_{NTR})_{LW} + (\Delta^i C_{NTR})_{WW} \\
(\Delta^i C_{NTR})_{\substack{LW \\ WW}} &= \pm[c\bar{\xi}_{TR}(\alpha)/l][\xi_{TR}(\alpha) - \xi_{TR}(0)]C_p\,\P \\
\Delta^i C_{mTR} &= (\Delta^i C_{mTR})_{LW} + (\Delta^i C_{mTR})_{WW} \\
\Delta^i C_{mTR} &= -\Delta^i C_{NTR}[\bar{\xi}_{TR}(\alpha) - \xi_{CG}] \\
\bar{\xi}_{TR}(\alpha) &= [\xi_{TR}(\alpha) + \xi_{TR}(0)]/2 \\
\xi_{TR}(\alpha) &= (l/c)x\begin{cases}[x_{TR}(\alpha)/l] : [x_{TR}(\alpha)/l] \leqq 1 \\ 1 \quad\quad : [x_{TR}(\alpha)/l] > 1\end{cases} \\
C_p &= 2\Delta v_{TR}(M_e^2 - 1)^{-1/2} \\
\Delta v_{TR} &= (\partial\delta^*/\partial x)_{TURB} - (\partial\delta^*/\partial x)_{LAM}
\end{aligned}\right\} \quad (11)$$

The definition of $\bar{\xi}_{TR}(\alpha)$ in Eq. (11) is a good approximation for a slender cone (θ_c small). For the data in Fig. 2, Eq. (11) gives the results shown in Fig. 4, which have a striking similarity to those shown in Fig. 3.** The contribution from the windward side is clearly negligible. As the leeward side transition movement is linear in (α/θ_c) for the $(\Delta\alpha/\theta_c)$-range of interest[13] (Fig. 2), one can define the stability derivative simply as $\Delta^i C_{m\alpha TR} = (\Delta^i CmTR)_{LW}/\Delta\alpha$. Equation (11) gives

$$\Delta^i C_{m\alpha TR} = [\Delta C_{mTR}/(l/c)^2 C_p](\Delta v/\Delta\alpha)2\cot^2\theta_c/(M_e^2 - 1)^{1/2} \quad (12)$$

¶ Plus-sign for leeward side, minus-sign for windward side.

** The "appropriate" $x_{TR}(0)/l$-scale is shown together with Ward's original $R_{l\infty}$-scale.

The displacement-thickness-slope-difference Δv_{TR} is obtained from Mangler-transformed flat-plate values.[20,21] For $R_{xTRe} = 5 \times 10^6$

$$\Delta v_{TR^0} = 0.04(M_e - 5) + \Delta v_{TR}(5) \quad (13)$$

where $\Delta v_{TR}(5) = 0.15$ for $T_W/T_{ST} = 0.25$, a typical tunnel value,[10] and $\Delta v_{TR}(5) = 0.23$ for $T_W = T_{AW}$.

Equations (12) and (13) give for $\theta_c = 10°$ and $\Delta\alpha = 1.8°$, $\Delta^i C_{m\alpha TR}/[\Delta C_{mTR}/(l/c)^2 C_p] = 1.10$–$1.54$ for $M_{\infty} = 6$, and $= 0.90$–1.02 for $M_{\infty} = 5$. This brings the data in Figs. 3 and 4 into quantitative agreement. The maximum transition-induced effect $(\Delta^i C_{m\alpha})_{\max}$ (Fig. 3) measured by Ward[4] agrees rather well with the predictions from Eqs. (11–13) (Fig. 5).

Measurements in the same tunnel of a more slender cone show similar results[5] (Fig. 6). The same oscillation amplitude, $\Delta\alpha \approx 2°$, was used, but the relative amplitude, $\Delta\alpha/\theta_c$, was roughly twice as large as in the case of the 10° cone. Consequently, the maximum statically destabilizing transition effects occur twice as early (compare Figs. 4 and 7). Figure 8 shows the maximum transition-induced effect $(\Delta^i C_{m\alpha})_{\max}$. The slope $\partial[x_{TR}(\alpha)/x_{TR}(0)]/\partial(\alpha/\theta_c)$ was obtained from Fig. 6 of Ref. 13.

The boundary-layer growth on the leeside meridian is influenced by the time history of the upstream boundary-layer

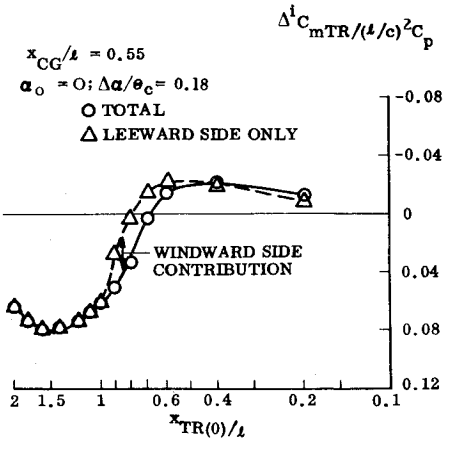

Fig. 4 Transition-induced moment on a 10° sharp cone at low hypersonic speeds.

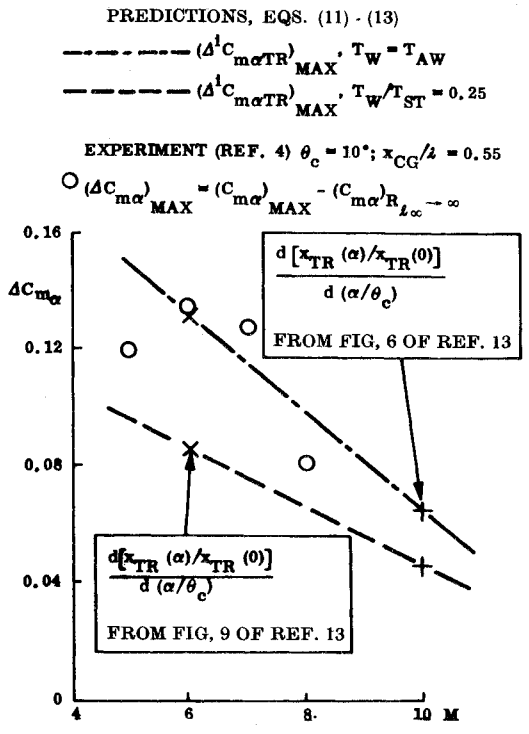

Fig. 5 Maximum transition-induced static stability increment on a sharp 10° cone.

influx,[22] an effect that is present already at infinitesimally small angles of attack.[23] If one lumps the upstream crossflow effects at x_1, the unsteady boundary-layer thickness at x_{TR} on the leeward meridian (of the aft body) can be expressed as follows:

$$\delta(x_{TR}, t) = (\delta)_{\substack{\alpha=0\\ \dot{\alpha}=0}} + \frac{\partial\delta}{\partial\alpha}\tilde{\alpha}(x_1, t-\Delta t) \qquad (14)$$

$\tilde{\alpha}$ is the angular representation of body crossflow, given by

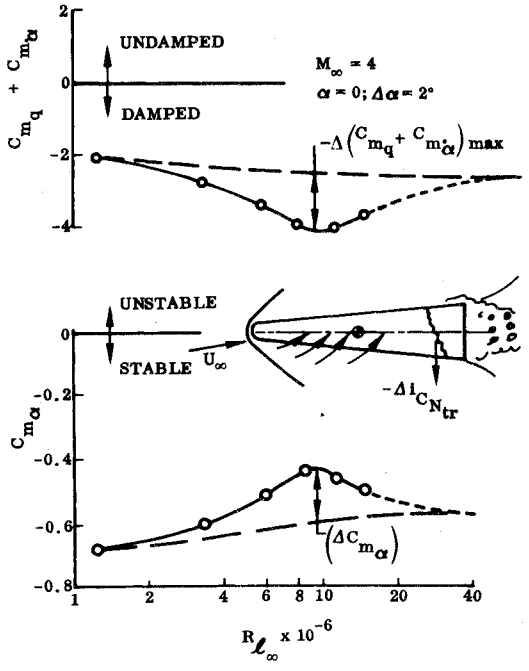

Fig. 6 Maximum transition-induced static stability increment on a blunted slender cone.

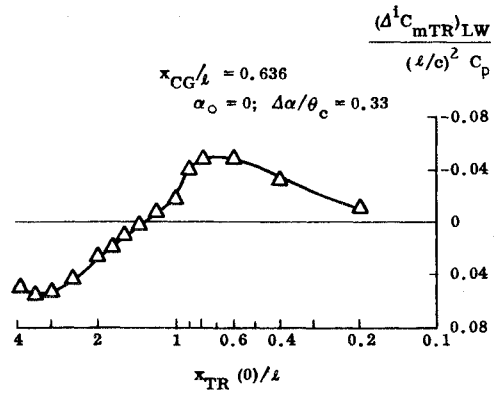

Fig. 7 Transition-effects on blunted cone stability characteristics.

Eq. (5),†† and Δt is the time increment occurring before a change of body crossflow at x_1 has resulted in changed boundary-layer thickness at x_{TR}. For the typically slow oscillations of a re-entry body (see discussion of Eq. (7) earlier), $\bar{\omega}^2 \ll 1$, and

$$\tilde{\alpha}(t-\Delta t) = \tilde{\alpha}(t) - \Delta t\dot{\tilde{\alpha}}(t) \qquad \Delta t = (x_{TR}-x_1)/\bar{U} \qquad (15)$$

$\bar{U}$ is the boundary-layer convection velocity, $\bar{U}/U_e \leqq 1.0$. Thus, the transition-induced leeside‡‡ force $\Delta^i C_{NTR}$ can be written as follows:

$$\Delta^i C_{NTR} = \Delta^i C_{NTR}(\alpha_0) + [\partial\Delta^i C_{NTR}/\partial\delta](\partial\delta/\partial\alpha) \times \{\theta + [(\xi_1 - \xi_{c.g.}) - (\xi_{TR} - \xi_1)/(\bar{U}/U_e)]\}(c\dot{\theta}/U_e) \qquad (16)$$

For finite amplitudes, ξ_{TR} in Eq. (16) has to be substituted by $\bar{\xi}_{TR}(\alpha)$, as defined in Eq. (11). The following derivatives are defined by Eq. (16)

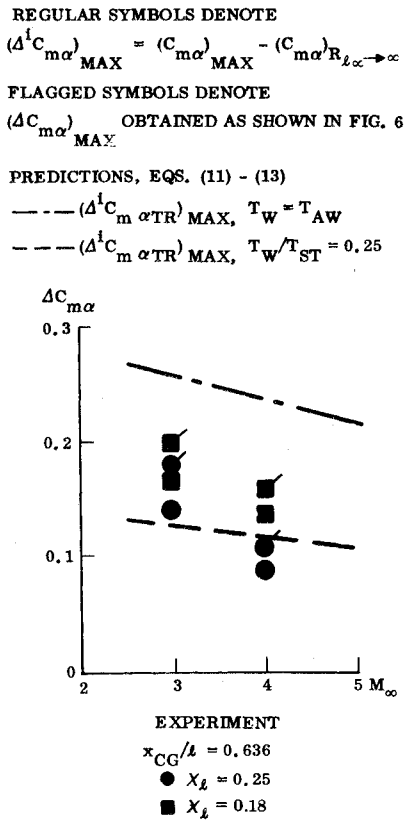

Fig. 8 Transition-induced moment on a 6° blunted cone at low hypersonic speeds.

†† For rigid body.

‡‡ The windward side boundary-layer crossflow effect is negligible for a sharp cone, as has been discussed earlier (Fig. 4).

$$\partial\Delta^i C_{NTR}/\partial\theta = (\partial\Delta^i C_{NTR}/\partial\delta)(\partial\delta/\partial\alpha) = \Delta^i C_{N\alpha TR}$$

$$\partial\Delta^i C_{NTR}/\partial(c\dot{\theta}/U_\infty) = \Delta^i C_{N\dot{\alpha}TR} = \Delta^i C_{N\alpha TR}[(\xi_1-\xi_{c.g.})-(\bar{\xi}_{TR}-\xi_1)/(\bar{U}/U_e)]/(U_e/U_\infty) \quad (17)$$

With $\Delta C_{mTR} = -(\bar{\xi}_{TR}-\xi_{c.g.})\Delta C_{NTR}$, Eq. (17) gives

$$[\Delta^i(C_{mq}+C_{m\dot{\alpha}})_{TR}/(\Delta^i C_{m\alpha})_{TR}]_{LW} = (\Delta^i C_{N\dot{\alpha}TR})_{LW}/(\Delta^i C_{N\alpha TR})_{LW} = [(\xi_1-\xi_{c.g.})-(\bar{\xi}_{TR}-\xi_1)/\bar{U}/U_e)](U_e/U_\infty) \quad (18)$$

For a slender sharp cone $\bar{U}_e/U_\infty = 1$. For a blunted cone U_e/U_∞ is defined at hypersonic speeds simply through embedded Newtonian theory[24]

$$U_e/U_\infty = 0.68+0.42\chi^{1/2} \quad (19)$$

With $\xi_1 < \xi_{c.g.} < \bar{\xi}_{TR}$ Eq. (18) shows that asymmetric aft body transition effects exhibit the same reversal in regard to the influence on static and dynamic stability as the aft body symmetric transition effects, Eq. (10). However, in the case of aft body leeside transition effects, the static stability is decreased and the dynamic stability increases; i.e., the effects are opposite to what they were for symmetric aft body transition on an ablating body [see Eq. (10)]. This reversal is also exhibited by the experimental data (Figs. 3 and 6). Figure 9 shows that this boundary-layer buildup effect has difficulty accounting for all the dynamic amplification measured on both the blunted cone and the sharp cone. The boundaries for the predictions using Eq. (18) were obtained as follows: the low boundary is for $\bar{U}/U_e = 1.0$, $\bar{\xi}_{TR} = \bar{\xi}_{TR}(\alpha)$, and $\xi_1 = (\xi_{AC})$ forebody. The high boundary is obtained with $\bar{U}/U_e = 0.8$, $\bar{\xi}_{TR} = l/c$, and $\xi_1 = \xi_0$. It can be shown that the dynamic quantity $(C_{mq}+C_{m\dot{\alpha}})$, the effective damping factor extracted from a dynamic test at finite amplitudes, is weighted heavily by the infinitesimal amplitude damping derivative $C_{m\dot{\theta}}$ existing at $\tilde{\alpha} = 0$, where the angular rate $\dot{\theta}$ is the maximum.[24] In that case, i.e., at $\tilde{\alpha} = 0$, $|C_{m\dot{\theta}}|$—maximum is obtained for maximum $\bar{\xi}_{TR}$, i.e., for $\bar{\xi}_{TR} = l/c$. It is somewhat harder to justify the forward x_1-limit, $x_1 = x_0$, used for the high estimate, especially for the sharp cone. This is a change from the earlier analysis,[5] which will be discussed in detail.

In the earlier analyses[5,41] essentially only the low limit was shown for the sharp cone, and the remaining 50% of the measured amplification was ascribed to accelerated flow effects and possible sting interference. A careful examination of available data showed that sting interference was not likely to have influenced the measurements.[41] Morkovin points out[25,26] that the effect of accelerated flow (favorable pressure gradient) on transition is a very nebulous quantity at hypersonic speeds and therefore cannot supply a good physical explanation for the large dynamic amplification measured on the sharp cone. As all experimental data demonstrate that the leeward side transition is totally dominated by crossflow effects,[13] it was natural to examine further the earlier choice of x_1 for the lumped forebody crossflow effects.

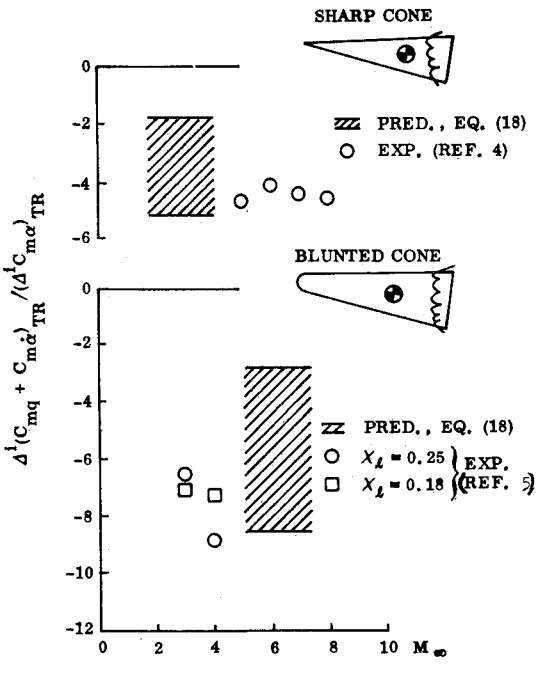

Fig. 9 Comparison between predicted and measured dynamic amplification of transition-induced static stability changes on sharp and highly blunted cones.

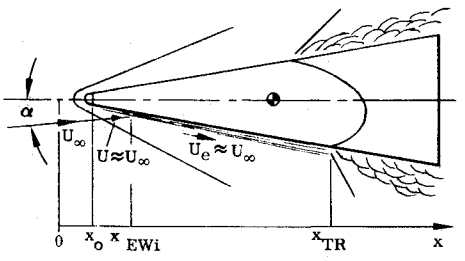

Fig. 10 Definitions for windward side transition.

The earlier choice, x_1 = forebody aerodynamic center, makes sense only if transition occurs owing to near-wall flow-shear. This is true for subsonic and transonic speeds when the stabilizing effect of accelerated flow is also well documented. However, at hypersonic speeds transition is caused by the flow-shear near the boundary-layer edge, not near the wall. This is the prime reason for losing the transonic pressure gradient effects. For the same reason, boundary-layer crossflow near the transition location, which only changes the near-wall velocity profile, should have little effect on transition. It is the upstream boundary-layer buildup near the nose that makes up the outer boundary layer on the downstream leeward side. Thus, lumping the upstream boundary-layer crossflow effects to a station near the nose tip makes more sense in hypersonic flow than lumping them to the forebody aerodynamic center. This is also in agreement with the nose-dominance in the case of mass addition effects.[27] Thus, the upper limit for the prediction is much closer to a realistic estimate, as is also indicated by the experimental data. It is also consistent with expectations to find the high limit, i.e., $x_1 = x_0$, to be more realistic for the blunted cone than for the sharp cone. (Figure 9 shows the high limit to overshoot the experimental data for the sharp but not for the blunted cone.)

The windward side asymmetric transition effects are negligible when the cone is sharp or nearly so, and also when the nose bluntness is very large, as for the cone discussed (Figs. 7–9). However, for intermediate nose bluntness, the entropy-impingement/entropy-swallowing effects cause appreciable windward side transition movement, although it is less in magnitude than the leeward side transition movement (Fig. 4 of Ref. 13). With the definitions in Fig. 10 the transition-induced forces on the windward side of a slender cone with moderately small nose bluntness can be written

$$\left.\begin{aligned}\Delta^i C_{NTR_{WW}} &= [\Delta^i C_{NTR}(\alpha_0)]_{WW}+(\partial\Delta^i C_{NTR}/\partial\delta)\times(\partial\delta/\partial\alpha)\tilde{\alpha}(\xi_0, t-\Delta t_{WW})\\ \Delta t_{WW} &= (c/U_\infty)[\xi_{EWi}-\xi_0+(\bar{\xi}_{TR}-\xi_{EWi})/(\bar{U}/U_e)]\end{aligned}\right\} \quad (20)$$

The following derivatives for the windward side transition effects are defined by Eqs. (15) and (20)

$$\left.\begin{aligned}\partial(\Delta^i C_{NTR})_{WW}/\partial\theta &= (\Delta^i C_{N\alpha TR})_{WW}\\ \partial(\Delta^i C_{NTR})_{WW}/\partial(c\dot{\theta}/U_\infty) &= (\Delta^i C_{N\dot{\alpha}TR})_{WW} = -(\Delta^i C_{N\alpha TR})_{WW}[\xi_{CG}+\xi_{EWi}-2\xi_0+(\bar{\xi}_{TR}-\xi_{EWi})/(\bar{U}/U_e)]\end{aligned}\right\} \quad (21)$$

The windward side transition effect has a larger dynamic amplification factor than the leeward side effect. Equation (21) gives

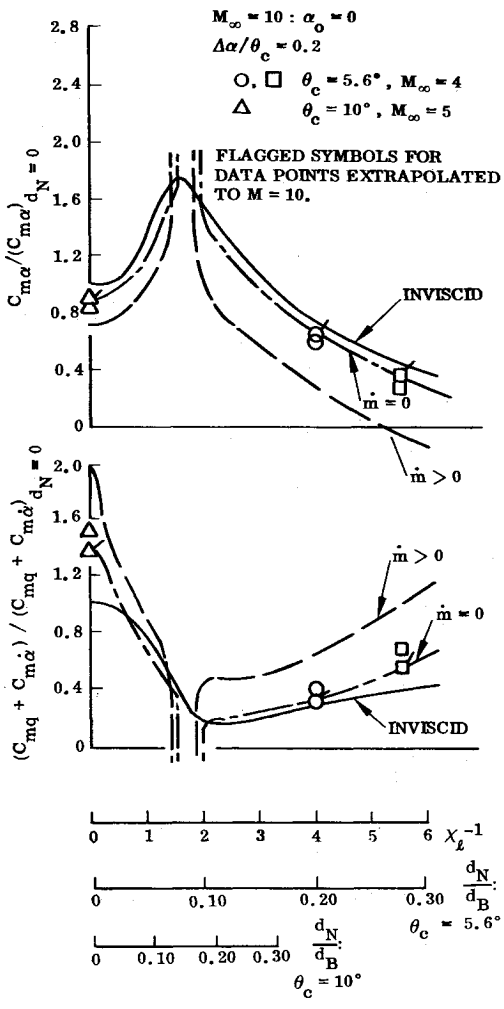

Fig. 11 Combined effects of nose bluntness and transition on slender cone stability derivatives.

$$[\Delta^i(C_{mq}+C_{m\dot{\alpha}})_{TR}/(\Delta^i C_{m\alpha})_{TR}]_{ww} = (\Delta^i C_{N\dot{\alpha}TR})_{ww}/(\Delta^i C_{N\alpha TR})_{ww} = -[(\xi_{c.g.}+\xi_{EWi}-2\xi_0)+(\bar{\xi}_{TR}-\xi_{EWi})/(\bar{U}/U_e)] \quad (22)$$

As $\xi_0 \ll \xi_{EWi}$ the ratio given by Eq. (22) is almost twice as large as that given by Eq. (18) for the leeside transition effect. Experiments show that the α-slope for the windward side transition movement is almost half of that for the leeside transition effect.[13] One can therefore expect the combined asymmetric transition effects on moderately blunt nonablating cones to have a very small effect on the dynamic stability and mainly cause a loss of static stability. However, if the nose bluntness is in the critical range, a dramatic loss of dynamic stability can result[28] (Fig. 11).

The discussion of asymmetric transition effects has been limited to nonablating vehicles until now. When transition takes place on an ablating conic frustum, two new effects have to be considered, viz., the increase of boundary-layer thickness upstream of transition, and the relative change of the self-induced pressures aft of transition owing to local mass addition effects. The latter effect is covered under the symmetric transition effects discussed earlier. Unless the mass addition rates are very high, these ablation-induced forces are small compared to those generated by the transition front movement with unchanged self-induced pressures. That is, the main influence of ablation on the asymmetric transition effect is the increased forebody boundary-layer thickness and associated increased transition-sensitivity to attitude changes. As long as the attitude and oscillation amplitude are small compared to the cone half-angle, the forebody mass addition rate can be assumed constant (at the value determined by θ_c). Thus the analytic techniques developed earlier for the nonablating vehicle are directly applicable. In fact, the forebody mass addition effect may be somewhat similar to the effect of increasing the Mach number; i.e., in both cases the boundary-layer displacement thickness is increased.

There are, of course, effects which have been neglected in the present treatment that would have to be considered in a more complete analysis, e.g., the effect of ablation-induced roughness and mass addition on the transition-behavior. On the windward side not only are the tripping effects of mass addition[10,29] and roughness[30,31] larger because the "tripping devices" are larger on the hotter windward side, but the thinner boundary layer on the windward side is also very much easier to trip than the leeward side thicker boundary layer.[30,32,33] It seems justified to neglect these coupling effects in a first approximation.

With the above assumptions a judicious use of hypersonic nose-bluntness-scaling[24] gives the hypothetical stability characteristics[28] shown in Fig. 11 for vehicles with asymmetric (aft body) transition. The data in Figs. 5 and 8 have been used to extrapolate to the hypersonic Mach number $M = 10$. For the ablating vehicle the effective nose bluntness is larger than for a nonablating vehicle,[11,34] causing an increase of the effective χ_l^{-1}. Forebody mass addition also steepens the entropy gradient, thus increasing the entropy wake-induced effects on the stability characteristics.[27] It should be emphasized that the curve for $\dot{m} > 0$ in Fig. 11 is hypothetical and not based on actual data.

Figure 11 is very instructive. It shows that asymmetric boundary-layer transition usually has an adverse effect on the vehicle stability characteristics, and that this adverse effect is amplified through ablative mass addition. On very blunt cones, which have marginal static stability, the asymmetric transition is statically destabilizing, and could jeopardize the static stability when an ablating heat shield is used to protect the conic (aft body) frustum. On moderately blunt cones which have marginal dynamic stability, the effect is dynamically destabilizing, and could possibly cause dynamic instability§§ for critical combinations of cone angle and nose bluntness.[28] The critical χ_l^{-1}-range depends on the relative amplitude $\Delta\alpha/\theta_c$. For zero amplitude a singular χ_l^{-1}-value is obtained. The data in Fig. 11 are all for zero (mean) angles of attack, i.e., $\alpha_0 = 0$. If one substitutes χ_l in Fig. 11 with $\bar{\chi}_l$ where $\bar{\chi}_l = \chi_l[1+(8/3\pi)(\alpha/\theta_c)]$, one could get a fairly representative picture for lifting re-entry, as $\bar{\chi}_l$ has been shown to scale the combined effects of nose bluntness, cone angle, and angle of attack, at least with the accuracy needed for a rough preliminary design estimate.[24]

Transition-Induced Trim Characteristics

So far only the transition effects on vehicle stability characteristics have been discussed. Since Nelson's pioneering work[36] the potentially dangerous effects of body asymmetries on the re-entry vehicle motion have been recognized, and the phenomenon as experienced by high-performance re-entry vehicles has been studied by numerous investigators.[37-39] Small mass asymmetries, with or without accompanying aerodynamic asymmetries, will cause the re-entry body to expose one roll-orientation on the body longer than others to a certain magnitude flow inclination.[40] The result may be a lasting nose asymmetry (Fig. 12a) or body bending through differential windward and leeward side thermal expansion (Fig. 13a). Both effects can cause body trim as well as attitude insensitive roll torques.[39]

Boundary-layer transition will amplify the nose asymmetry effect (Fig. 12). With the geometry sketched in Fig. 12a, the vehicle will trim at a certain angle of attack. As the nose-asymmetry-induced loading is almost a force couple,¶¶ the

§§ For an ablating vehicle this is likely to be true even when considering the dynamically stabilizing effect of the vehicle lift derivative (the drag effect is probably negligible).[35]

¶¶ For the particular nose bluntness chosen (for this very reason).

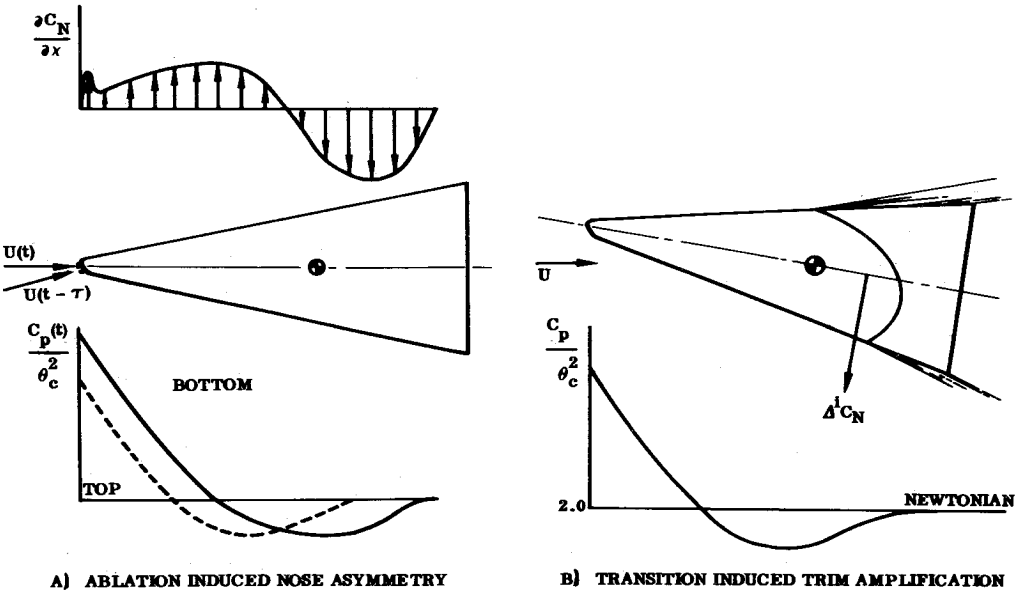

Fig. 12 Combined effects of asymmetric nose bluntness and transition on trim.

vehicle will trim at an angle of attack where the nose asymmetry induces no loads on the aft body; i.e., the entropy impingement occurs at the same distance (x_{EWi}) from the nose on both top and bottom sides (Fig. 12b). Because of the large boundary-layer crossflow effects, transition will occur earlier on the leeward side, producing a net negative aft body load and thereby increasing the trim caused by the nose asymmetry. Likewise, the force couple induced by body bending (in addition to the induced lift through body camber) will cause a trim which is amplified by boundary-layer transition (Fig. 13). The aft body bending response to the asymmetric heating induced by the transition will cause a trim in the opposite direction and could possibly reverse the (original) trim.

From all the data reviewed in the present paper, it is obvious that when transition first occurs on a vehicle that is not perfectly symmetric, aerodynamically ($\Delta\alpha = \alpha_0 = 0$) and otherwise, the transition will move forward asymmetrically. All indications are that this initial asymmetric transition movement forward will be very fast, almost jumpwise. If the nose bluntness is either very small or very large, this transition behavior would cause a nearly stepwise increase of the trim before it starts affecting the oscillatory stability derivatives.* This transient transition behavior would cause the $\bar{\alpha}$-envelope of a re-entry body to show a very fast divergence at the time of transition. Following this fast $\bar{\alpha}$-divergence would be an $\bar{\alpha}$-convergence at a higher rate than that existing before transition. [The asymmetric transition increases the damping for these nose-bluntness values (Fig. 11).] Disregarding this transient behavior and lumping the total $\bar{\alpha}$-envelope divergence into a damping derivative could produce unrealistic, high levels of negative damping. For nose bluntnesses not falling in the above region, i.e., for critical χ_l-values in Fig. 11, the $\bar{\alpha}$-divergence would be a bona fide negative damping effect. Even then the levels of the negative damping would be large, especially initially before peak $\bar{\alpha}$ is reached. However, this behavior would persist over several cycles of pitch-oscillation, and, in addition, the following $\bar{\alpha}$-convergence would be much slower than in the previous case. This description of $\bar{\alpha}$-envelope behavior is still very speculative and is based on hypothetical data such as that displayed in Fig. 11. Additional theoretical and experimental work is needed before a quantitative description can be given of the full degree of freedom re-entry vehicle motion.

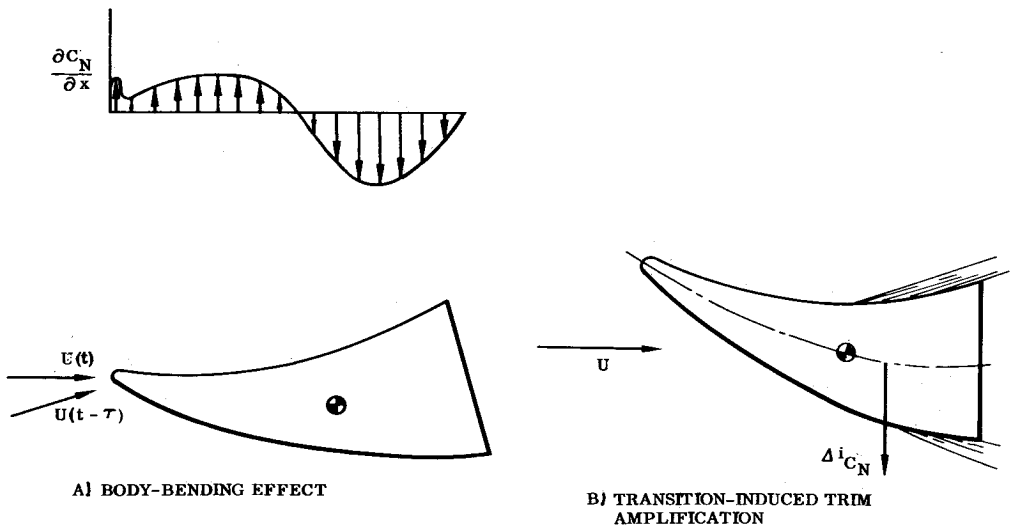

Fig. 13 Combined effect of body bending and transition.

* If the flight data were of unusual completeness and quality, one would be able to distinguish this as a trim buildup.

Conclusions

The results of a review of transition effects on slender vehicle stability and trim characteristics can be summarized as follows for aft body transition (i.e., mean transition aft of body c.g.).

The effect of transition on stability and trim characteristics can be predicted using the experimental correlations of transition-movement with relative angle of attack (α/θ_c) in a simple analytic theory. The agreement with experimentally observed transition effects on static and dynamic stability derivatives is fairly good for the limited amount of dynamic experimental data available.

The effect of symmetric transition, i.e., the axial position of the centroid of the transition front, is negligible compared to the effect of asymmetric transition, i.e., the axial extent of the windward and leeward side transition fronts. This is always true in regard to the static characteristics. It is also true for the dynamic characteristics, provided that the thermodynamic time-lag is not unusually large.

Transition aggravates the adverse stability effects of nose bluntness, decreasing dynamic stability for moderately blunt vehicles, which already have marginal dynamic stability, and decreasing static stability of vehicles with large nose bluntness, where static rather than dynamic stability is the problem.

Transition also aggravates the adverse trim effects of nose asymmetry and body bending.

In summary, the effects of transition are always adverse, both in regard to stability and trim characteristics for ballistic re-entry. For lifting re-entry, the trim effect of transition could well be within the control capability required for other reasons, and the dynamic effects would be relatively small, provided the critical χ_l-region is avoided; i.e., d_N/d_B, θ_c, α_0, and $\Delta\alpha$ are chosen such that negative damping will not occur.

Additional theoretical and experimental work is required before slender vehicle stability and trim characteristics at time of transition can be predicted with the desired accuracy and confidence level. However, the results revealed by a review of presently existing information indicate that the prospects for the development of such a theoretical capability in the near future are bright, contrary to what seemed to be the widespread opinion at the time of the review.

References

[1] Sacks, I. and Schurmann, E. E., "Aerodynamic Phenomena Associated With Advanced Reentry Systems," AVCO-RAD-TM-63-79, Oct. 1963, pp. 18–22, Avco Corp., Wilmington, Mass.

[2] Grimes, J. H., Jr. and Casey, Y. Y., "Influence of Ablation on the Dynamics of Slender Re-entry Configurations," *Journal of Spacecraft and Rockets*, Vol. 2, No. 1, Jan.–Feb. 1965, pp. 106–108.

[3] Ericsson, L. E. and Reding, J. P., "Ablation Effects on Vehicle Dynamics," *Journal of Spacecraft and Rockets*, Vol. 3, No. 10, Oct. 1966, pp. 1476–1483.

[4] Ward, L. K., "Influence of Boundary Layer Transition on Dynamic Stability at Hypersonic Speeds," Paper 6, *Transactions of the 2nd Technical Workshop on Dynamic Stability Testing*, Arnold Air Force Station, Tenn., April 20–22, 1965.

[5] Ericsson, L. E., "Effect of Boundary-Layer Transition on Vehicle Dynamics," *Journal of Spacecraft and Rockets*, Vol. 6, No. 12, Dec. 1969, pp. 1404–1409.

[6] Martelucci, A. and Neff, R. S., "The Influence of Asymmetric Transition on Re-Entry Vehicle Motion," *Journal of Spacecraft and Rockets*, Vol. 8, No. 5, May 1971, pp. 476–482.

[7] Martellucci, A., "Asymmetric Transition Effects on the Static Stability and Motion History of a Slender Vehicle," SAMSO TR-70-141, 1970, Space and Missiles Systems Organization, Los Angeles Air Force Base, Calif.

[8] Softley, E. J., Graber, B. C., and Zempel, R. C., "Experimental Observation of Transition of the Hypersonic Boundary Layer," *AIAA Journal*, Vol. 7, No. 2, Feb. 1969, pp. 257–263.

[9] Stetson, K. F. and Rushton, G. H., "A Shock Tunnel Investigation of the Effects of Nose Bluntness, Angle of Attack, and Boundary-Layer Cooling on Boundary-Layer Transition at a Mach Number of 5.15," *AIAA Journal*, Vol. 5, No. 5, May 1967, pp. 899–906.

[10] DiChristina, V., "Three Dimensional Laminar Boundary-Layer Transition on a Sharp 8° Cone at Mach 10," *AIAA Journal*, Vol. 8, No. 5, May 1970, pp. 852–856.

[11] Laganelli, A. L. and Martellucci, A., "Downstream Effects of Gaseous Injection Through a Porous Nose," AIAA Paper 72-185, San Diego, Calif., 1972.

[12] Martellucci, A., Chaump, L., Rogers, D., and Smith, D., "Experimental Determination of the Aero-Acoustic Environment about a Slender Cone," *AIAA Journal*, Vol. 11, No. 5, May 1973, pp. 635–642.

[13] Ericsson, L. E., "Correlation of Attitude Effects on Slender Vehicle Transition," to be published (see also Ref. 41 below).

[14] Ames Research Staff, "Equations, Tables and Charts for Compressible Flow," R 1135, 1953, NACA.

[15] Tanner, D. D., "Simulation of the Compressible Turbulent Boundary Layer With Air Injection," TM 55-21-56, LMSC-806354, Contract AF 04(694)-814, Oct. 1966, Lockheed Missiles & Space Co., Sunnyvale, Calif.

[16] Kratsch, K. M., Hearne, L. F., and McChesney, H. R., "Theory for the Thermophysical Performance of Charring Organic Heat-Shield Composites," Rept. LMSC-803099, Oct. 1963, with Addendum by Lefferdo, J. M., "Sublimer: Thermal Response of a Low Temperature Sublimer—A computer Program," TIAD 840, Aug. 22, 1966, Lockheed Missiles & Space Company, Inc., Sunnyvale, Calif.

[17] Collosimo, D. D., "The Effects of Mass Transfer on the Dynamic Stability of Slender Cones," Rept. 141, May 1965, Cornell Aeronautical Lab., Buffalo, New York.

[18] Moore, D. R., Stalmach, D. J., Jr., Pope, T. C., and Jenkins, J. E., "Dynamic Stability Wind Tunnel Tests of a 10° Cone with Simulated Ablation at $M = 17$," *AIAA Journal*, Vol. 5, No. 8, Aug. 1967, pp. 1377–1385.

[19] Intieri, P. F., Kirk, D. B., Chapman, G. T., and Terry, J. E., "Ballistic Range Tests of Ablating and Nonablating Slender Cones," *AIAA Journal*, Vol. 8, No. 3, March 1970, pp. 558–564.

[20] Schlichting, H., *Boundary Layer Theory*, 4th ed., McGraw-Hill, New York, 1960.

[21] Eckstrom, P. J., "Engineering Analysis of Boundary Layers and Skin Friction on Bodies of Revolution of Zero Angle of Attack," TM 55-21-21, LMSC-805162, May 1965, Lockheed Missiles & Space Co., Inc., Sunnyvale, Calif.

[22] Tracy, R. R., "Hypersonic Flow over a Yawed Circular Cone," GALCIT Memo 69, 1963, California Institute of Technology, Pasadena, Calif.

[23] Moore, F. K., "Laminar Boundary Layer on a Cone in Supersonic Flow at Large Angle of Attack," TN 2844, 1952, NACA.

[24] Ericsson, L. E., "Effect of Nose Bluntness, Angle of Attack, and Oscillation Amplitude on Hypersonic Unsteady Aerodynamics of Slender Cones," *AIAA Journal*, Vol. 9, No. 2, Feb. 1971, pp. 297–304.

[25] Morkovin, M. V., "Open Questions—Transitions to Turbulence at High Speeds, 1971," Paper 9a, Vol. III, *Proceedings of the Boundary Layer Transition Workshop*, Rept. TOR-0172(S2816-16)-5, Nov. 3–5, 1971, The Aerospace Corp., San Bernardino, Calif.

[26] Morkovin, M. V., "Critical Evaluation of Transition from Laminar to Turbulent Shear Layers with Emphasis on Hypersonically Traveling Bodies," AFFDL-TR-68-149, March 1969, Air Force Flight Dynamics Lab., Wright-Patterson Air Force Base, Ohio.

[27] Ericsson, L. E. and Guenther, R. A., "Dynamic Instability Caused by Forebody Blowing," *AIAA Journal*, Vol. 11, No. 2, Feb. 1973, pp. 231–233.

[28] Ericsson, L. E., "Transition Effects on Vehicle Dynamics and Accuracy," Paper 3, Vol. I, *Proceedings of the Boundary Layer Transition Workshop*, Rept. TOR-0172 (S2816-16)-5, Nov. 3–5, 1971, The Aerospace Corp., San Bernardino, Calif.

[29] Marvin, J. G. and Akin, C. M., "Combined Effects of Mass Addition and Nose Bluntness on Boundary-Layer Transition," *AIAA Journal*, Vol. 8, No. 5, May 1970, pp. 857–863.

[30] McCauley, W. D., Saydah, A. R., and Bueche, J. F., "Effect of Spherical Roughness on Hypersonic Boundary-Layer Transition," *AIAA Journal*, Vol. 4, No. 12, Dec. 1966, pp. 2142–2148.

[31] Whitfield, J. D. and Lannuzzi, F. A., "Experiments on Roughness Effects on Cone Boundary-Layer Transition Up to Mach 16," *AIAA Journal*, Vol. 7, No. 3, Mar. 1969, pp. 465–470.

[32] Young, C. H., Reda, D. C., and Roberge, A. M., "Hypersonic Transitional and Turbulent Flow Studies on a Lifting Entry Vehicle," *Journal of Spacecraft and Rockets*, Vol. 10, No. 12, Dec. 1972, pp. 883–888.

[33] Pate, S. R. and Adams, J. C., "Hypersonic Simulation for Lifting Body Transition Studies," Paper 6, Vol. III, *Proceedings of the Boundary Layer Transition Workshop*, Rept. TOR-0172(S2816-16)-5, Nov. 3–5, 1971, The Aerospace Corp., San Bernardino, Calif.

[34] Ericsson, L. E., "Universal Scaling Laws for Hypersonic Nose Bluntness Effects," *AIAA Journal*, Vol. 7, No. 12, Dec. 1969, pp. 2222–2227.

[35] Nelson, R. L., "Measurement of Aerodynamic Characteristics of Reentry Configurations in Free Flight at Hypersonic and Near-Orbital Speeds," AGARD Rept. 380, July 1961.

[36] Nelson, R. L., "The Motions of Rolling Symmetrical Vehicles Referred to a Body Axis System," TN 3737, 1956, NACA.

[37] Kanno, J. S., "Spin Induced Forced Resonant Behavior of a Ballistic Body Reentering the Atmosphere," Rept. LMSD-238139, Vol. 3, Jan. 1960, Lockheed Missiles & Space Div., Sunnyvale, Calif.

[38] Pettus, J. J., "Persistent Re-Entry Vehicle Roll Resonance," AIAA Paper 66-49, New York, N.Y., 1966.

[39] Price, D. A., Jr., "Sources, Mechanisms, and Control of Roll Resonance Phenomena for Sounding Rockets," *Journal of Spacecraft and Rockets*, Vol. 4, No. 11, Nov. 1967, pp. 1516–1525.

[40] Price, D. A., Jr. and Ericsson, L. E., "A New Treatment of Roll Pitch Coupling for Ballistic Reentry Vehicles," *AIAA Journal*, Vol. 8, No. 9, Sept. 1970, pp. 1608–1615.

[41] Ericsson, L. E., "Transition Effects on Slender Vehicle Stability and Trim Characteristics," AIAA Paper 73-126, Washington, D.C., 1973.

JANUARY 1974 J. SPACECRAFT VOL. 11, NO. 1

Experimental Wake Flow Properties of a Viking '75 Entry Vehicle

JAMES F. CAMPBELL* AND CLARENCE A. BROWN JR.†
NASA Langley Research Center, Hampton, Va.

An experimental investigation has been conducted to obtain the flow properties in the wake of a model of the blunt Viking '75 entry vehicle. Data are presented for the model at several angles of attack at freestream Mach numbers from 0.2 to 3.95. The characteristics of the wake flowfield are discussed and results are shown to demonstrate the significant variation of wake centerline flow properties in the transonic speed range, the shift in wake profiles with change in angle of attack, and the similarity exhibited by the velocity profiles across the wake.

Nomenclature

b = value of z that corresponds to $(V_\infty - V_1)/(V_\infty - V_{1_{CL}}) = 0.50$
D = maximum diameter of model of Viking entry vehicle
M = Mach number
q = dynamic pressure
V = velocity
X, Y, Z = inertial axis system
x, y, z = distances along X, Y, Z axes
α = angle of attack of model centerline

Subscripts
1 = local flow property
CL = property value on wake centerline
∞ = freestream flow property
stag = value at wake stagnation point

Introduction

NASA'S goals of planetary exploration have resulted in a program to land an unmanned, instrumented payload on Mars. This program has been designated as Viking '75 and is scheduled to commence with a launch in mid-1975 for an encounter with Mars in mid-1976. Research on the atmospheric properties of Mars have indicated the surface pressure to be on the order of 5–10 mbars, a thin atmosphere compared to our Earth's surface pressure of about 1000 mbars. Because of this low pressure, the unmanned spacecraft has a low ballistic coefficient and utilizes an auxiliary decelerating force to land. The deceleration system selected for the Viking '75 entry vehicle is a large diameter parachute. Such a parachute, together with the low ballistic coefficient of the entry vehicle, will provide the necessary aerodynamic deceleration required to traverse the Martian atmosphere and enable the spacecraft to soft land.

The selection of an aerodynamic drag-producing parachute deployed aft of a forebody requires a knowledge of the flow structure of the wake. This information is fundamental in any attempt to estimate parachute inflation-drag and -stability characteristics, drag efficiency, and structural loading. Because the flowfields behind bodies, especially blunt bodies, are extremely difficult to model analytically,[1–5] experimental tests are usually performed to provide the desired information. References 6–11 illustrate some of the studies that have been conducted to experimentally define the flow properties of wakes behind a variety of bodies. In response to initial design studies related to the Viking mission, a comprehensive wind-tunnel investigation was undertaken to measure the flowfields aft of the large-angle cone type of blunt body.[12–14] During this study, wake data were obtained for a preliminary version of the Viking '75 entry vehicle with freestream Mach numbers from 0.20 to 3.95.[15–17]

The purpose of the current paper is to summarize the experimental results in order to evaluate the characteristics of the flowfield aft of the Viking '75 entry vehicle for a wide range of freestream Mach numbers. In addition, the effects on the wake resulting from changing vehicle angle of attack are also considered.

Experimental Arrangement

The wake survey was performed using a pressure rake located aft of a model of a preliminary configuration of the Viking '75 entry vehicle (see Fig. 1). The basic component of the model was a 140° cone which had a spherical nose radius of 0.25 D in addition to a small shoulder radius at the point of maximum diameter (D). This model also had an afterbody in the base region composed of frustums of two cones. The current configuration of the Viking '75 entry vehicle has slight differences in the nose radius and afterbody section from the model used in this wake evaluation.

Two wind-tunnel facilities at the NASA Langley Research

Presented as Paper 73-475 at the AIAA 4th Aerodynamic Deceleration Systems Conference, Palm Springs, Calif., May 21–23, 1973; submitted May 14, 1973; revision received July 30, 1973.

Index categories: Jets, Wakes, and Viscid-Inviscid Flow Interactions; Viscous Nonboundary-Layer Flows.

* Aerospace Engineer. Associate Fellow AIAA.

† Aerospace Engineer. Member AIAA.